中国科学院新疆天文台
XINJIANG ASTRONOMICAL OBSERVATORY, CAS

# Interstellar scintillation and polarization of PSR B0355+54 from FAST

Speaker: Jumei Yao

XAO pulsar group

2023/07/04

# Outline

1. PSR B0355+54 and its PWN

2. The scintillation of PSR B0355+54 from FAST

3. The polarization of PSR B0355+54 from FAST

4. Summary

Based FAST observations:

PSR B1842+14 and B1929+10, ISS arc detection, RAA, Yao et al. 2020;
PSR J0538+2817 and SNR S147, ISS and polarization, NA, Yao et al. 2021;
PSR B0656+14 and Monogem ring, ISS and polarization, ApJ, Yao et al. 2022;
PSR B0355+54 and its PWN, ISS and polarization, Yao et al. in prep.

# PSR B0355+54 and its PWN

- **The basic parameters of PSR B0355+54**

| NAME | | PSRJ | | PMRA (mas/yr) | | | PMDEC (mas/yr) | | | PX (mas) | | | Gl (deg) | Gb (deg) |
|---|---|---|---|---|---|---|---|---|---|---|---|---|---|---|
| B0355+54 | mth72 | J0358+5413 | mth72 | 9.3 | 5 | lwy+16 | 8.3 | 8 | lwy+16 | 0.91 | 16 | ccv+04 | 148.190 | 0.811 |

| DM (cm^-3 pc) | | | RM (rad m^-2) | | | DIST (kpc) | DIST_A (kpc) | | | AGE (Yr) | VTRANS (km/s) |
|---|---|---|---|---|---|---|---|---|---|---|---|
| 57.1420 | 3 | js06 | 81.5 | 3 | npn+20 | 1.000 | 1.0 | 0 | vwc+12 | 5.64e+05 | 59.10 |

(1) The distance of PSR B0355+54: 1000+/-200 pc (VLBI - PX, Verbiest et al. 2012)

(2) The transverse velocity of PSR B0355+54: 59+/-12 km/s (Li et al. 2016)

(3) The position angle of the transverse velocity: 48.3+/-3.2 deg (Li et al. 2016)

(4) The position angle of the spin axis: -33+/-5 deg (Carr P., 2007, PhD thesis, Univ. Manchester)

(5) The 2D spin-velocity angle: 25+/-6 deg (Li et al. 2016, Carr P., 2007)

# PSR B0355+54 and its PWN

- **The PWN of PSR B0355+54**

Noel Klingler et al. 2016

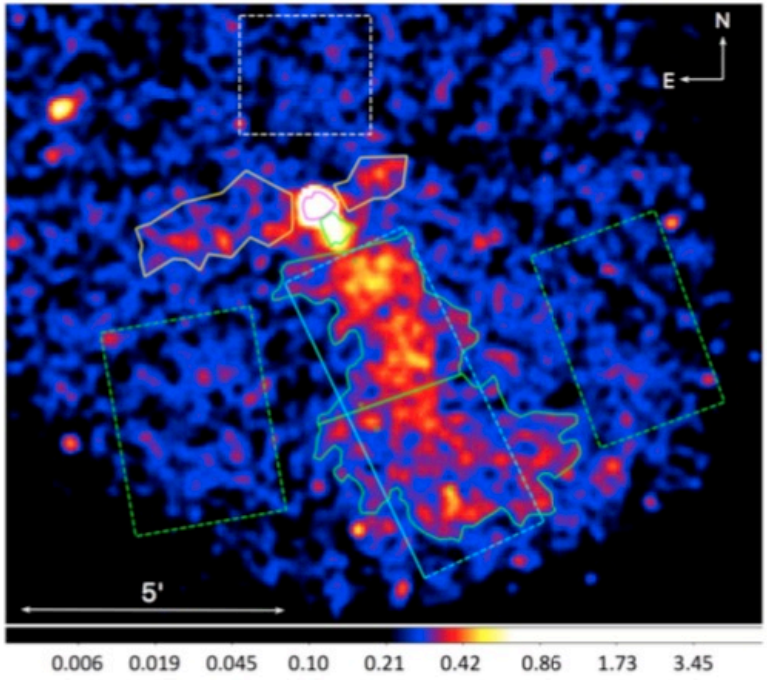


**Figure 2.** Merged 0.5–8 keV exposure-corrected image produced from all eight ACIS-I observations with point sources (detected by `wavdetect`) removed. The image is binned by a factor of eight (3.″9 pixel size), and smoothed with an $r = 11.''8$ Gaussian kernel. The following spectral extraction regions are shown: the tail (green contour region; the line separates the "near" and "far" halves), and the "whiskers" (yellow polygons on either side of the CN). The two green dashed rectangles to the sides of the tail are the background regions used in the tail's spectral fits. The cyan $2.'5 \times 6.'2$ rectangular region (along the tail contour) is used to extract the tail brightness profile (see Figure 5). The CN (magenta polygon) and stem (green polygon) are also shown (same regions as in Figure 2), along with the background region (dashed white box) used in the pulsar, CN, stem, and whiskers spectral fits. The level for the green contour was chosen in such a way that it conforms to the tail morphology at the contrast shown. The color bar is in units of counts arcsec$^{-2}$.

Chandra X-ray Observatory observations of PSR B0355+54:

(1) Long tail - about 2 pc

(2) As they found that the emission at the CN apex becomes distinguishable from the background at a distance of 3.5 arc-second in front of the pulsar, they guess that the projected stand-off radius is :

$$r_{0,\perp} \simeq 5.4 \times 10^{16} d_{1.04} \text{ cm}$$

The bow-shock is located about **0.02 pc** from the pulsar .

No Halpha observation

# PSR B0355+54 and its PWN

- **Interstellar scattering and scintillation**

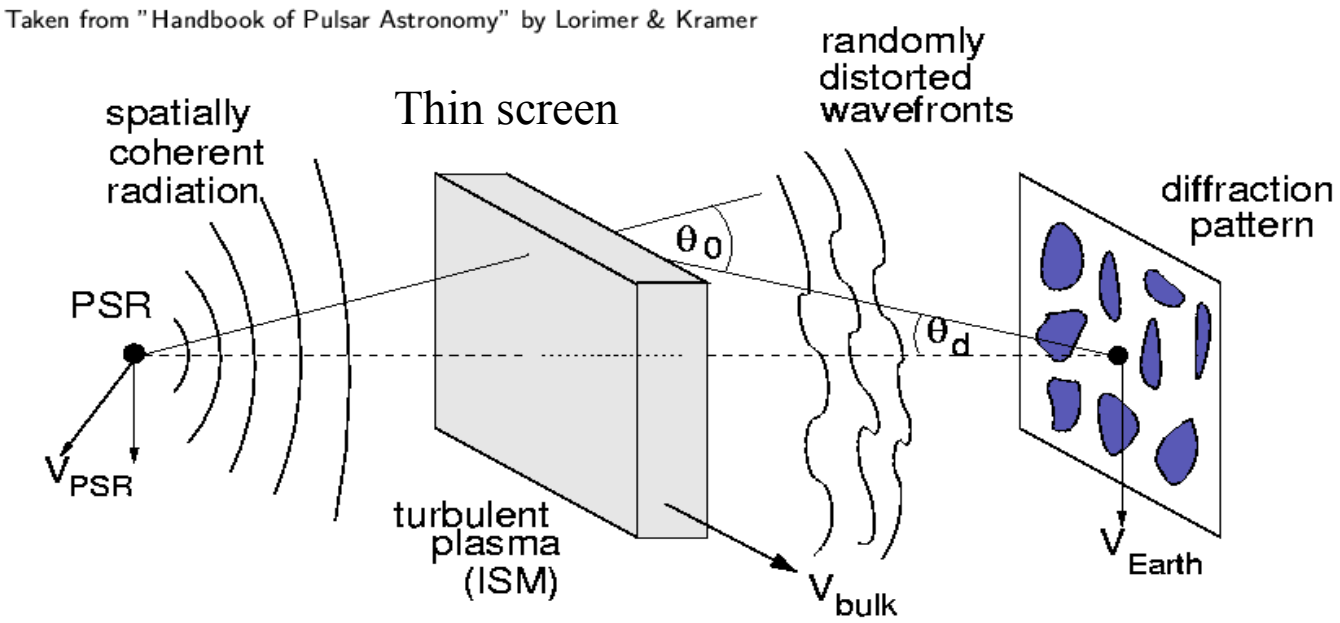


1. Scatter-broadened image and scattering tail

The geometric time delay $\Delta t(\theta) = \dfrac{\theta^2 d}{c}$

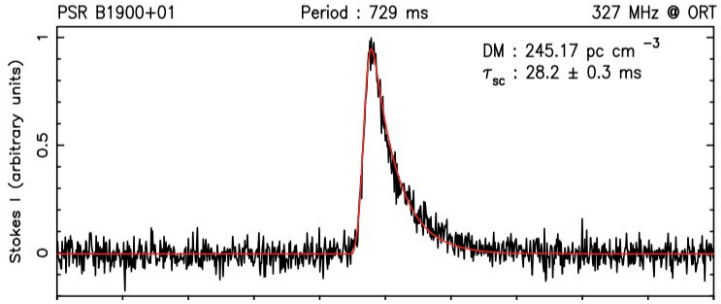


2. Scintillation (DS: Time and Freq; SS: arc)

$$f_\nu = \eta f_t^2 \qquad \eta = 4625 \frac{D_{\rm kpc}\, s(1-s)}{\nu^2_{\rm GHz} |V_{\rm eff,\perp}|^2}$$

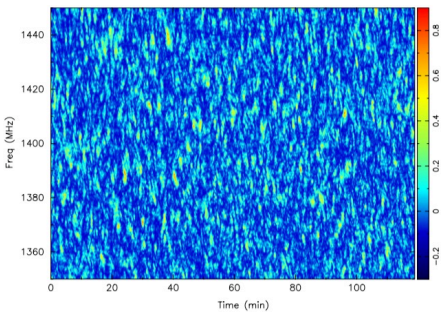


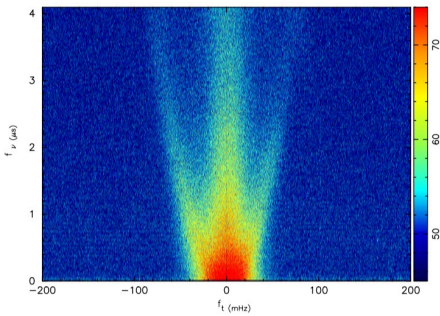

# PSR B0355+54 and its PWN

- **Interstellar scintillation of PSR B0355+54 from other telescopes**

(1)ISS arc detection for the first time at 1.4 GHz

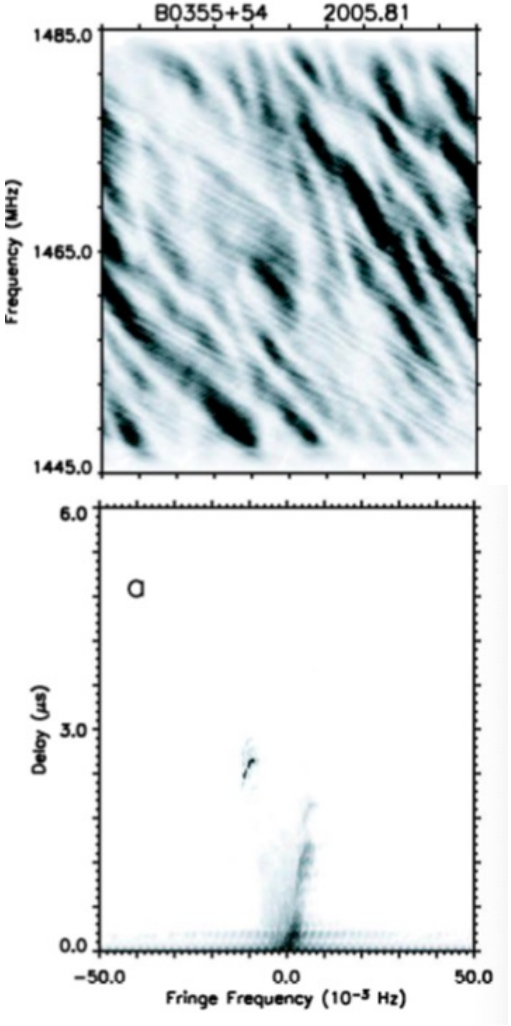


Dan Stinebring et al. 2006 (GBT)

(2) ISS arc detection at 2.2 GHz (curvature variation)

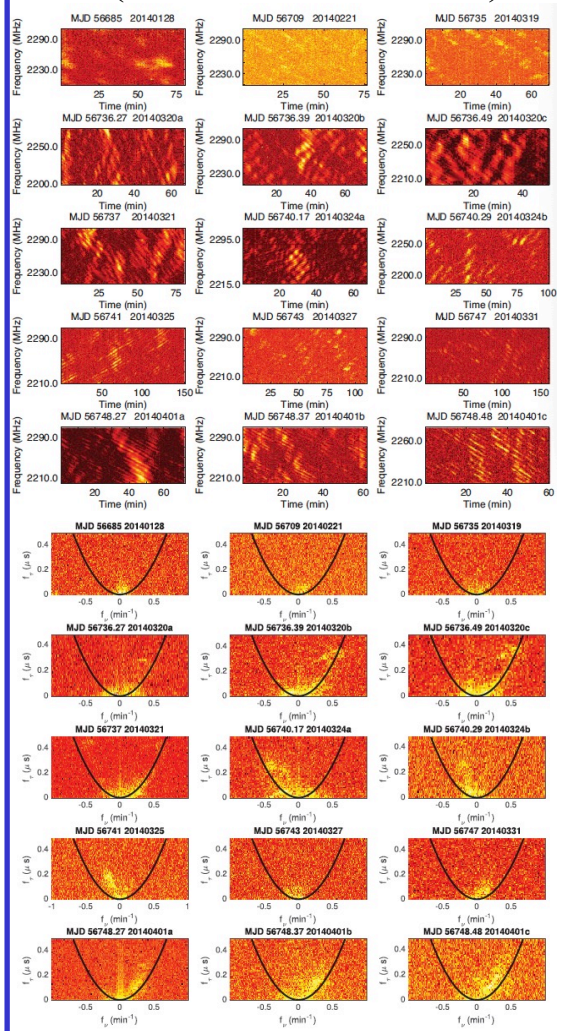

Xu et al. 2018 (Kunming 40 m)

(3) ISS arc detection at 2.2 GHz (arclets)

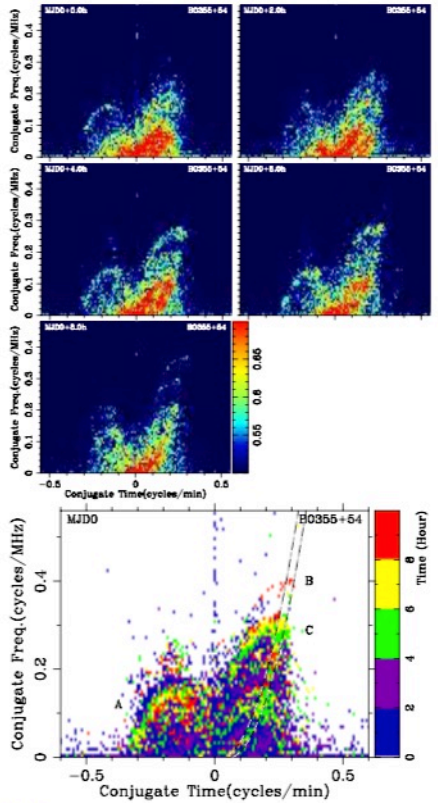


Fig. 17. *Upper five panels:* secondary spectra of PSR B0355+54 for five 2-h blocks of data started at MJD0 = 57416.036 + 105 min, extracted from the 12-h observation session of 57416.036 (see Fig. 2). *Bottom panel:* evolving secondary spectra plotted only for the maximum power in the five 2-h blocks of data for each pixel. Different color scales are used to mark which block of data was used for the maximum power. Three special inverted arclets are labeled A, B, and C, and the main parabola is indicated by the dashed lines.

Wang et al. 2018 (Jiamusi 66 m)

# The scintillation of PSR B0355+54 from FAST

- **The DS and ACF results**

1.1 GHz

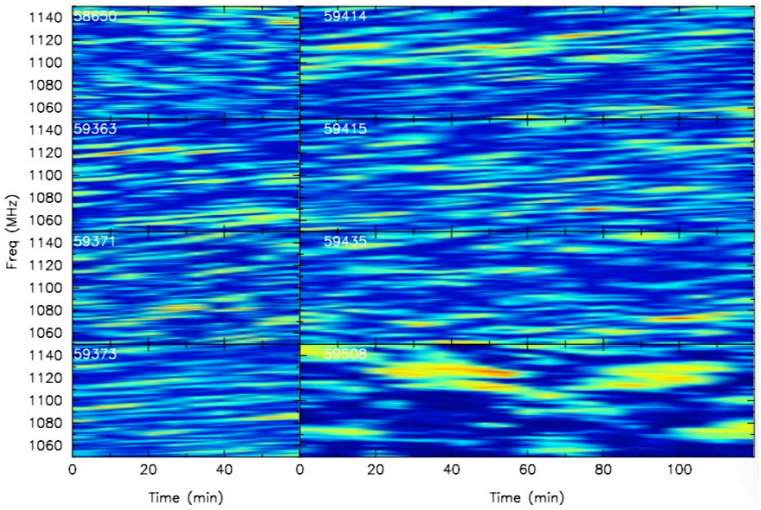


1.4 GHz

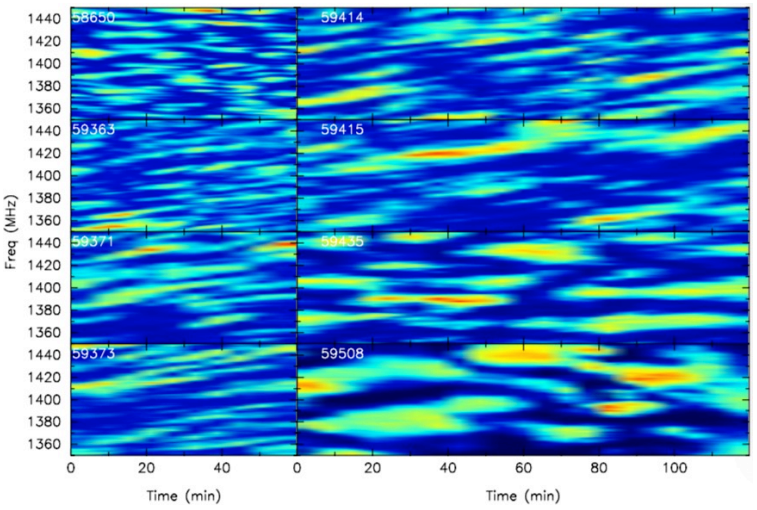


**Table 1.** The scintillation timescale and scintillation bandwidth at 1100 and 1400 MHz.

| MJD | A | $\Delta t_d$ | $\Delta \nu_d$ | A | $\Delta t_d$ | $\Delta \nu_d$ |
|---|---|---|---|---|---|---|
| | | 1100 MHz | | | 1400 MHz | |
| 58650 | 1.013±0.002 | 5.75±(0.02+0.05) | 0.80±(0.01+0.03) | 1.027±0.006 | 5.72±(0.04+0.27) | 1.72±(0.04+0.08) |
| 59363(C) | 1.017±0.006 | 5.77±(0.05+0.42) | 2.72±(0.02+0.19) | 0.972±0.006 | 5.54±(0.05+0.40) | 2.85±(0.07+0.21) |
| 59371(C) | 1.045±0.021 | 3.21±(0.09+0.13) | 1.51±(0.03+0.06) | 1.034±0.010 | 5.05±(0.06+0.43) | 4.31±(0.07+0.37) |
| 59373(C) | 0.958±0.014 | 4.87±(0.09+0.25) | 1.61±(0.03+0.08) | 0.939±0.016 | 4.84±(0.11+0.40) | 4.31±(0.03+0.36) |
| 59414(C) | 0.998±0.003 | 5.77±(0.04+0.26) | 2.04±(0.02+0.09) | 0.963±0.009 | 6.44±(0.08+0.44) | 4.32±(0.07+0.29) |
| 59415(C) | 1.002±0.003 | 5.54±(0.02+0.20) | 1.37±(0.05+0.05) | 0.981±0.003 | 10.56±(0.06+1.25) | 8.07±(0.03+0.96) |
| 59435(C) | 0.948±0.013 | 8.06±(0.14+0.39) | 1.74±(0.04+0.08) | 0.947±0.006 | 13.82±(0.11+1.29) | 3.77±(0.14+0.35) |
| 59508(C) | 0.941±0.013 | 8.19±(0.15+0.65) | 4.68±(0.06+0.37) | 0.992±0.003 | 11.69±(0.05+1.26) | 6.01±(0.17+0.65) |
| 59881(C) | 0.945±0.014 | 3.03±(0.06+0.06) | 0.90±(0.02+0.02) | 9.771±0.006 | 3.18±(0.03+0.10) | 1.92±(0.03+0.06) |
| 59883(C) | 0.859±0.028 | 4.45±(0.19+0.10) | 0.70±(0.05+0.02) | 9.496±0.008 | 5.34±(0.06+0.30) | 3.60±(0.08+0.20) |

Scintillation timescale and bandwidth largely vary with observing time.

# The scintillation of PSR B0355+54 from FAST

- **The ISS arcs in the SS**

1.1 GHz

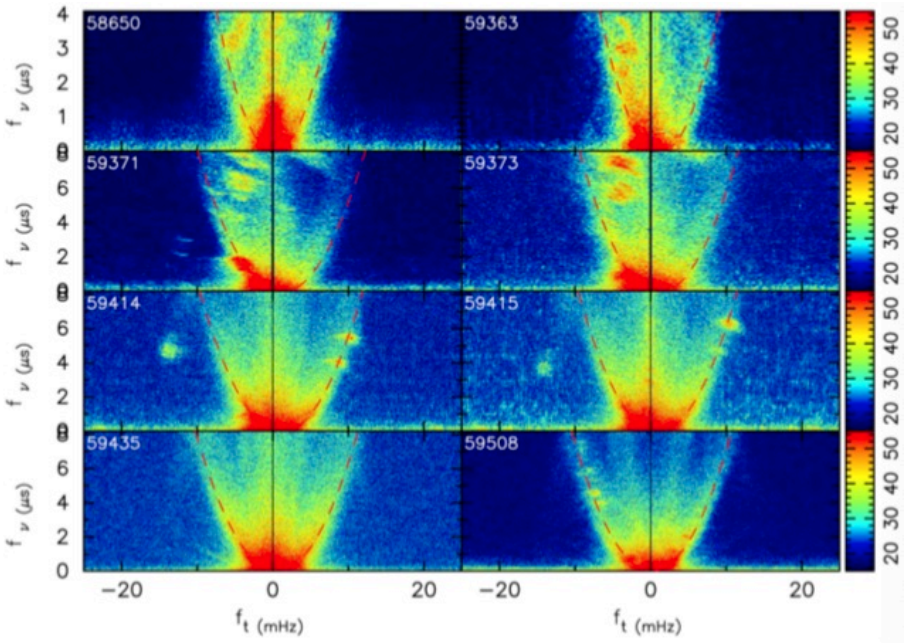


1.4 GHz

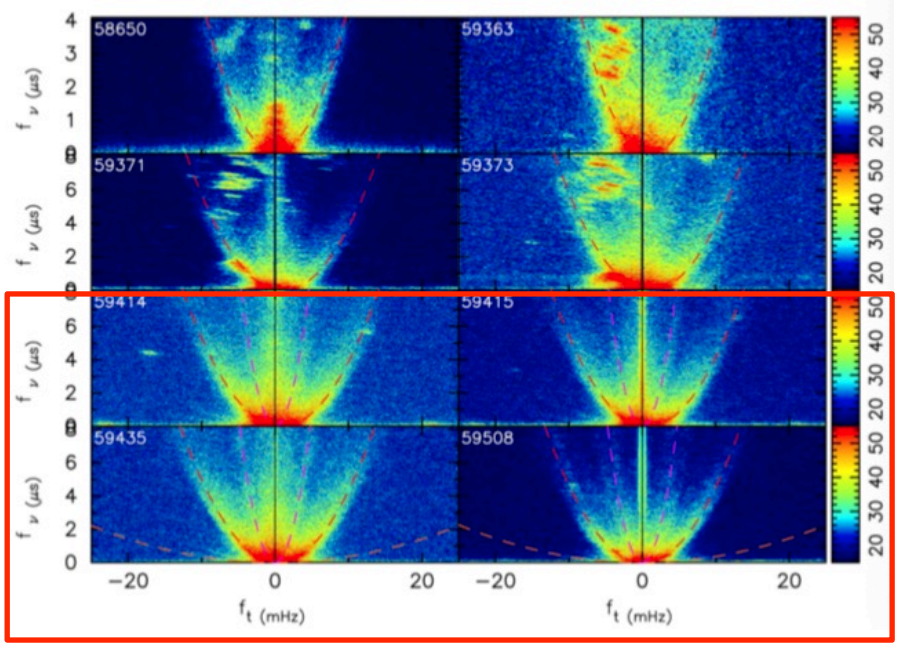


(1) One main ISS arc at 1.1 GHz, and three ISS arcs at 1.4 GHz;

(2) Small scale structures are located within the main arc;

(3) Small scale structures are located at the main arc;

(4) Small scale structures are located outside the main arc.

# The scintillation of PSR B0355+54 from FAST

- **The arc curvature at 1.1 and 1.4 GHz - two methods**

Arc b at 1.4 GHz ( power count)

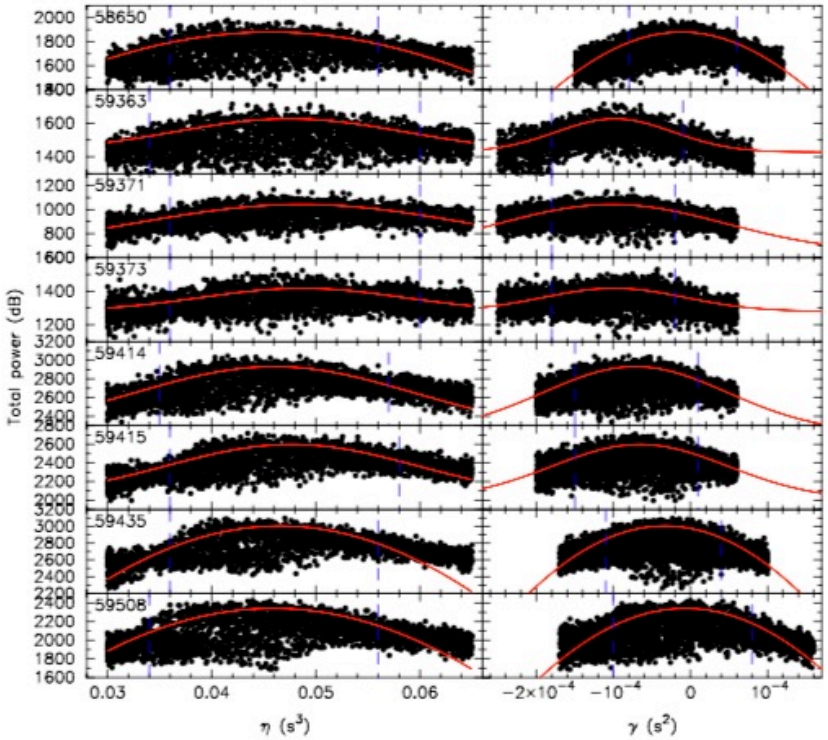


**Figure 4.** Curvature fit of arc b at 1400 MHz for the first eight epoches.

$$f_\nu = \eta f_t^2 + \gamma f_t$$

Arc a and c at 1.4 GHz (Normalize)

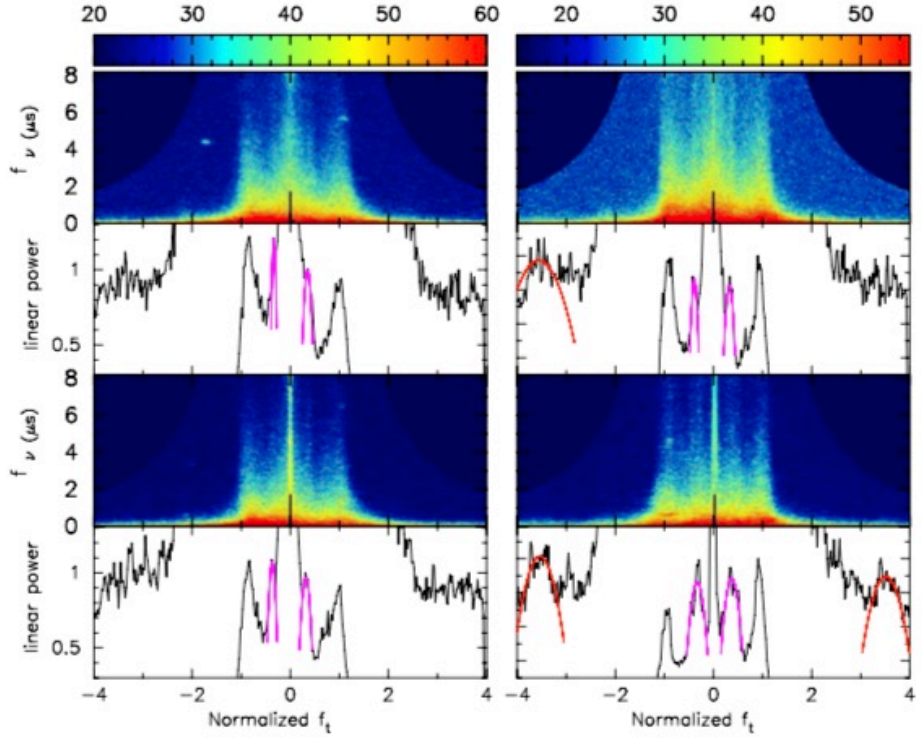


**Figure 5.** Curvature fit of arc a and c at 1400 MHz for MJDs 59414, 59415, 59435 and 59508.

$$f_\nu = \eta f_t^2$$

# The scintillation of PSR B0355+54 from FAST

- **The location of the scattering screen**

**Table 3.** The location of the scattering screens based on data at 1100 and 1400 MHz.

| MJD | $s_a$ | $D_{psa}$ pc | $s_b$ | $D_{psb}$ pc | $\theta_{gb}$ $\mu$as | $\Delta$DM $10^{-5}$pc cm$^{-3}$ | $\Delta$DM/AU $10^{-5}$pc cm$^{-3}$AU$^{-1}$ | ARb | $s_c$ | $D_{psc}$ pc |
|---|---|---|---|---|---|---|---|---|---|---|
| | | | | | 1100 MHz | | | | | |
| 58650 | | | 0.058±0.012 | 58±17 | −9.9±0.8 | ** | 0.70±0.06 | | | |
| 59363 | | | 0.055±0.012 | 55±16 | −65.4±3.4 | $DM_{ref}$ | 4.62±0.24 | | | |
| 59371 | | | 0.059±0.012 | 59±17 | −54.8±3.1 | 1.15±0.24 | 3.87±0.22 | | | |
| 59373 | | | 0.061±0.013 | 61±18 | −69.5±3.8 | 0.31±0.06 | 4.90±0.27 | | | |
| 59414 | | | 0.059±0.012 | 59±17 | −67.5±3.5 | 6.75±1.43 | 4.76±0.25 | | | |
| 59415 | | | 0.061±0.013 | 61±18 | −57.1±3.0 | 0.15±0.03 | 4.03±0.21 | | | |
| 59435 | | | 0.059±0.013 | 59±18 | −31.9±1.8 | 2.24±0.48 | 2.25±0.13 | | | |
| 59508 | | | 0.065±0.014 | 65±19 | −9.3±0.9 | 3.61±0.78 | 0.66±0.06 | | | |
| | | | | | 1400 MHz | | | | | |
| 58650 | | | 0.060±0.013 | 60±17 | −6.3±0.7 | ** | 0.72±0.08 | 7.9±1.2 | | |
| 59363 | | | 0.062±0.013 | 62±18 | −52.9±2.8 | $DM_{ref}$ | 6.05±0.32 | 3.9±0.9 | | |
| 59371 | | | 0.064±0.013 | 64±18 | −54.6±3.0 | 1.66±0.35 | 6.24±0.34 | 1.6±0.6 | | |
| 59373 | | | 0.064±0.013 | 64±18 | −53.2±3.2 | 0.43±0.09 | 6.08±0.36 | 1.4±0.6 | | |
| 59414 | | | 0.061±0.013 | 61±17 | −38.7±2.1 | 7.33±1.56 | 4.42±0.24 | 3.5±0.8 | 0.285±0.045 | 285±73 |
| 59415 | | | 0.063±0.013 | 63±18 | −35.4±1.9 | 0.15±0.03 | 4.05±0.22 | 5.4±1.8 | 0.287±0.045 | 287±73 |
| 59435 | 0.0053±0.0021 | 5.3±2.4 | 0.062±0.013 | 62±18 | −18.1±1.0 | 2.18±0.46 | 2.07±0.11 | 22.8±5.8 | 0.288±0.046 | 288±74 |
| 59508 | 0.0054±0.0013 | 5.4±1.7 | 0.066±0.014 | 66±18 | −3.3±1.3 | 3.04±0.68 | 0.38±0.15 | 9.8±2.9 | 0.288±0.066 | 288±88 |

$$\gamma = 0.1496 \frac{D_{\rm kpc}\theta_{g,mas}(1-s)}{\nu_{\rm GHz} V_{\rm eff,km/s}}$$

$$V_{\rm eff} = sV_E + (1-s)V_p - V_{\rm ISM}$$

$$\nabla\phi_{\parallel} = \theta_g * k = \theta_g * \frac{2\pi}{\lambda}$$

$$\Delta\phi(t) \approx \sum_{i=0}^{N(t)-1} \nabla\phi_{\parallel}(t_i) V_{\rm eff} * (t_{i+1} - t_i)$$

$$\Delta DM = -3.84 * 10^{-8} \nu \Delta\phi$$

(1) Arc a - 250 times stand-off radius (Not the bow shock);
(2) Arc b - seem like the SNR;
(3) Arc c - (Not the local hot bubble shell)

(4) Based on the refractive angle - we obtain the DM variations.

# The scintillation of PSR B0355+54 from FAST

- **The movement of the small scale structure - judge the origin**

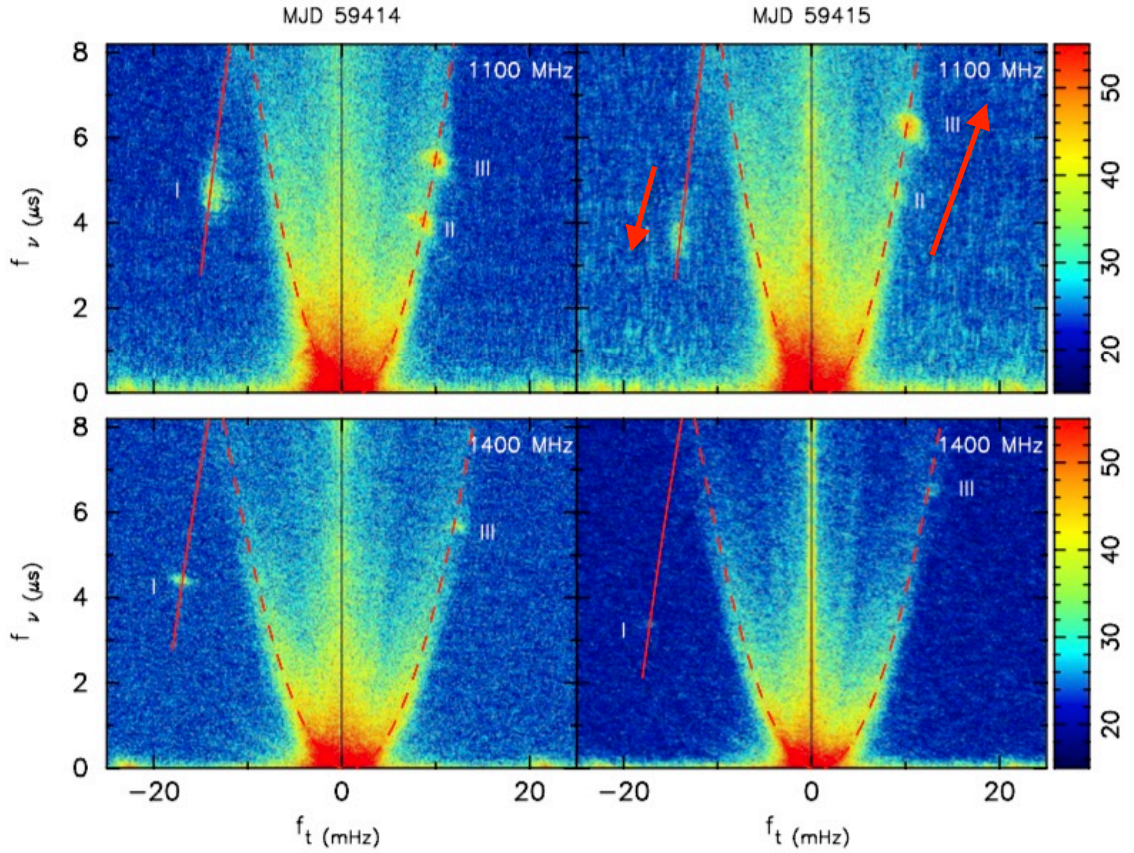


**Figure 11.** The movement of the II and III at 1100 and 1400 MHz.

(1) Structure I is located outside of the main arc;
(2) The moving direction of I is inconsistent with II and III.

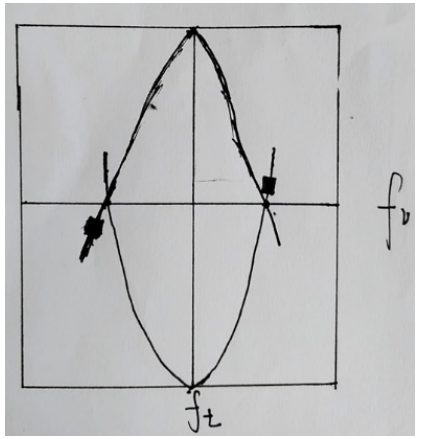


Explain I

**Table 5.** The movement of small structure I, II and III at 1100 and 1400 MHz.

| name and freq | $f_\nu$ μs | $\Delta f_\nu$ μs | $\theta$ μas | $\Delta\theta$ μas | a AU | $f_\nu$ μs | $\Delta f_\nu$ μs | $\theta$ μas | $\Delta\theta$ μas | a AU | V mas/yr |
|---|---|---|---|---|---|---|---|---|---|---|---|
| | MJD 59414 | | | | | MJD 59415 | | | | | |
| I (1100 MHz) | 11.6851±0.0102 | 1.21 | 860±123 | 277±40 | 0.26±0.06 | 12.7279±0.0161 | 0.94 | 898±135 | 244±37 | 0.23±0.06 | 13.7±66 |
| I (1400 MHz) | 11.9968±0.0109 | 0.42 | 854±130 | 160±24 | 0.15±0.04 | 13.0070±0.0141 | 0.27 | 899±136 | 130±20 | 0.12±0.03 | 16.3±68 |
| II(1100 MHz) | 3.9866±0.0097 | 0.59 | 534±72 | 205±28 | 0.19±0.05 | 4.6979±0.0184 | 0.48 | 570±82 | 182±26 | 0.17±0.04 | 13.0±40 |
| III(1100 MHz) | 5.4727±0.0058 | 0.50 | 612±84 | 185±25 | 0.17±0.04 | 6.2142±0.0075 | 0.86 | 646±94 | 240±35 | 0.22±0.06 | 12.3±46 |
| III(1400 MHz) | 5.6384±0.0022 | 0.38 | 598±90 | 155±23 | 0.15±0.04 | 6.5342±0.0143 | 0.46 | 648±97 | 172±26 | 0.16±0.04 | 18.0±48 |

$$f_\nu = \frac{D(1-s)}{2cs}(\theta^2 + 2\theta\theta_g)$$

**Consistent with pulsar proper motion**
**13 mas/yr**

# The scintillation of PSR B0355+54 from FAST

- **The observations at MJDs 59881 and 59883**

DS at 1.1 and 1.4 GHz

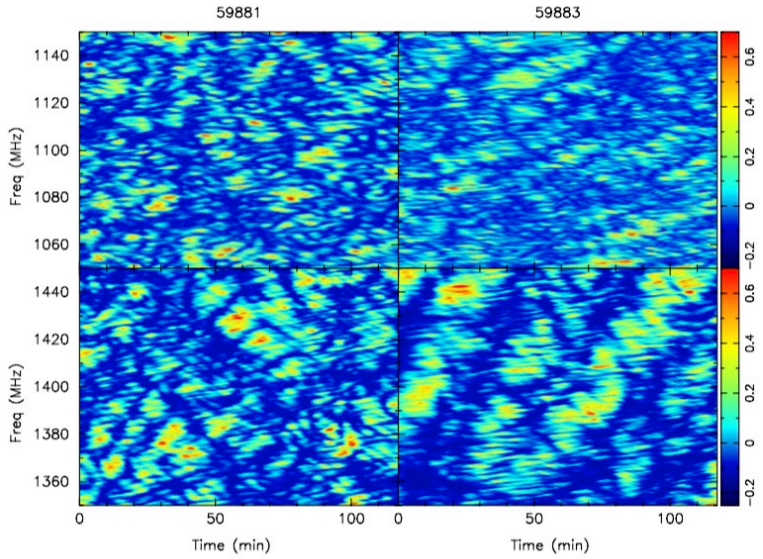


**Figure 14.** The dynamic spectra for the last two observations at 1100 and 1400 MHz.

SS at 1.1 and 1.4 GHz

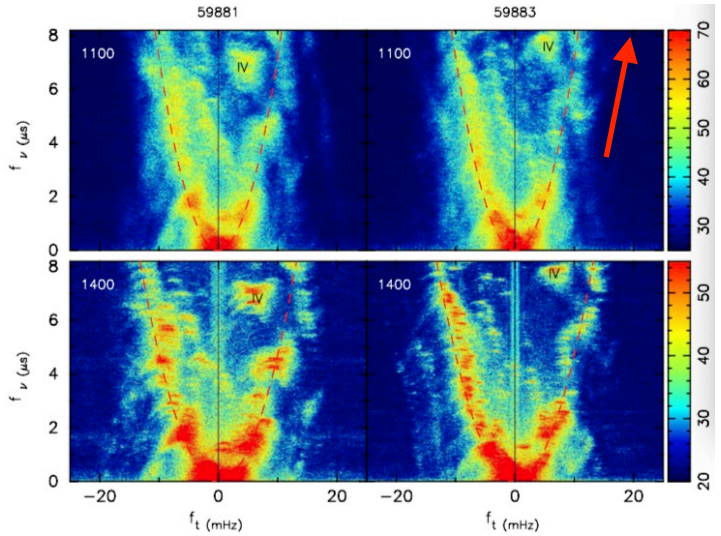


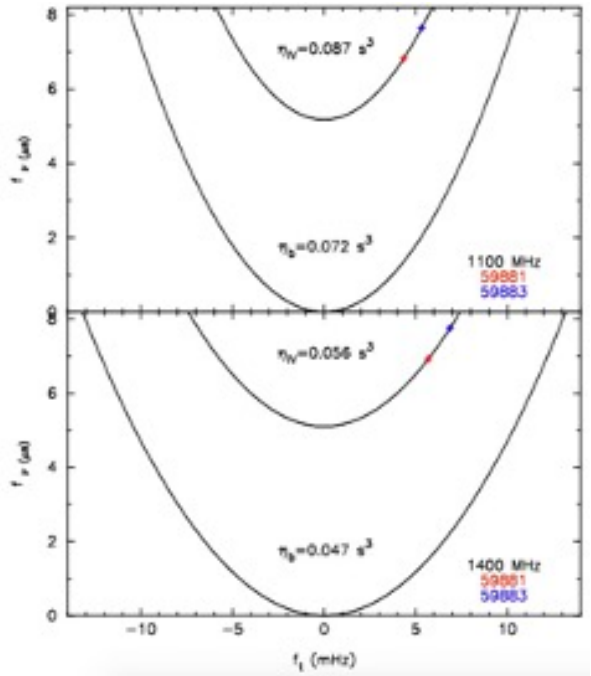


(1) Structure IV is located within the main arc;
(2) The moving direction of IV is consistent with that of II, III and the pulsar;
(3) The arc curvature of IV is larger than that of the main arc.

Where is IV coming from?

Can we simulate pulsar scattered image at these two days?

# The polarization of PSR B0355+54 from FAST

- **The mode change of PSR B0355+54 - Morris et al. 1980**

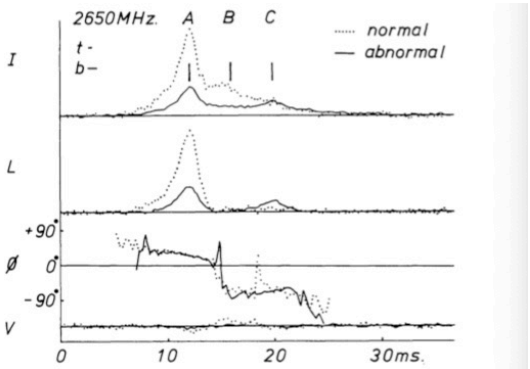


**Fig. 1.** Comparison of average pulse intensities and polarization for PSR 0355+54 in the normal (dotted) and abnormal (full line) modes. The smoothing due to interstellar dispersion ($b$) and the post detector time constant ($t$) are indicated. The curves, from top to bottom show total flux density ($I$), linearly polarized flux density ($L$), position angle of polarization ($\phi$), and ($V$) the circularly polarized component. (Right hand minus left.) The position of the windows $A$, $B$, and $C$ are shown

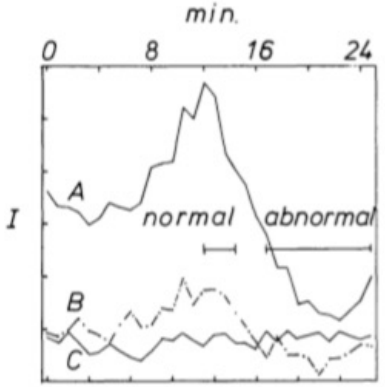


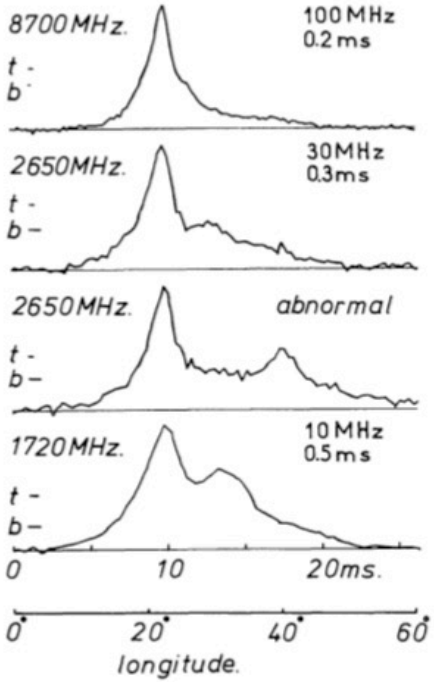


**Fig. 3.** Variation of the average pulse profile (Stokes parameter I) of PSR 0355+54 with observing radio frequency. The bandwidth and time constant are listed and the horizontal bars indicate the smoothing which results. The intensity scales have been arbitrarily adjusted to make the peak deflections equal on all four profiles. The zeroes of the longitude scales at 8,700 MHz and 1,720 MHz have been shifted to align the peaks with those of the 2,650 MHz profiles

Gradual mode change within 24 min and no PA change.

Pulse profiles vary with frequency; No mode change at other frequency.

# The polarization of PSR B0355+54 from FAST

- **The two modes from FAST (based on polarization)**

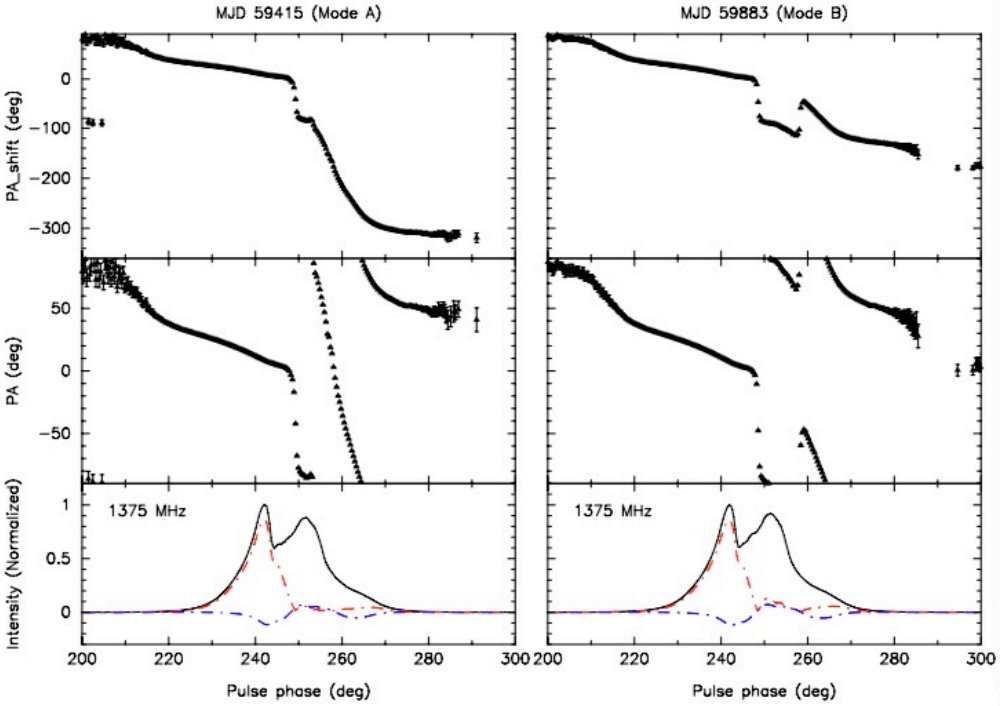


**Figure 18.** The observed PA at MJDs 59415 and 59883.

**Table 7.** Observed RM and the ionospheric and ISM contributions to it.

| MJD and UT | $RM_{obs}$ (rad. $m^{-2}$) | $RM_{iono}$ (rad. $m^{-2}$) | $RM_{ism}$ (rad. $m^{-2}$) | Mode |
|---|---|---|---|---|
| 59363 (UT 4 h) | 82.290±0.003 | | | B |
| 59371 (UT 2 h) | 82.187±0.001 | | | B |
| 59373 (UT 4 h) | 83.519±0.002 | | | A |
| 59414 (UT 1 h) | 83.106±0.002 | | | A |
| 59414 (UT 2 h) | 83.269±0.002 | | | A |
| 59415 (UT 1 h) | 82.800±0.003 | | | A |
| 59415 (UT 2 h) | 82.840±0.003 | | | A |
| 59435 (UT 22 h) | 81.959±0.002 | | | B |
| 59435 (UT 23 h) | 81.950±0.002 | | | B |
| 59870 (UT 17 h) | 81.938±0.002 | | | B |
| 59881 (UT 18 h) | 82.132±0.002 | | | B |
| 59881 (UT 19 h) | 82.095±0.002 | | | B |
| 59883 (UT 17 h) | 82.257±0.002 | | | B |
| 59883 (UT 18 h) | 82.058±0.002 | | | B |
| 59981 (UT 11 h) | 83.480±0.001 | | | B |
| 59981 (UT 12 h) | 83.289±0.001 | | | B |

(1) There are two modes based on the detected PA;
(2) The presence of both mode A and B have continuity in time;

(3) More analysis are needed next. ?????

# The polarization of PSR B0355+54 from FAST

- **The 2D spin-velocity angle (Based on Mode B)**

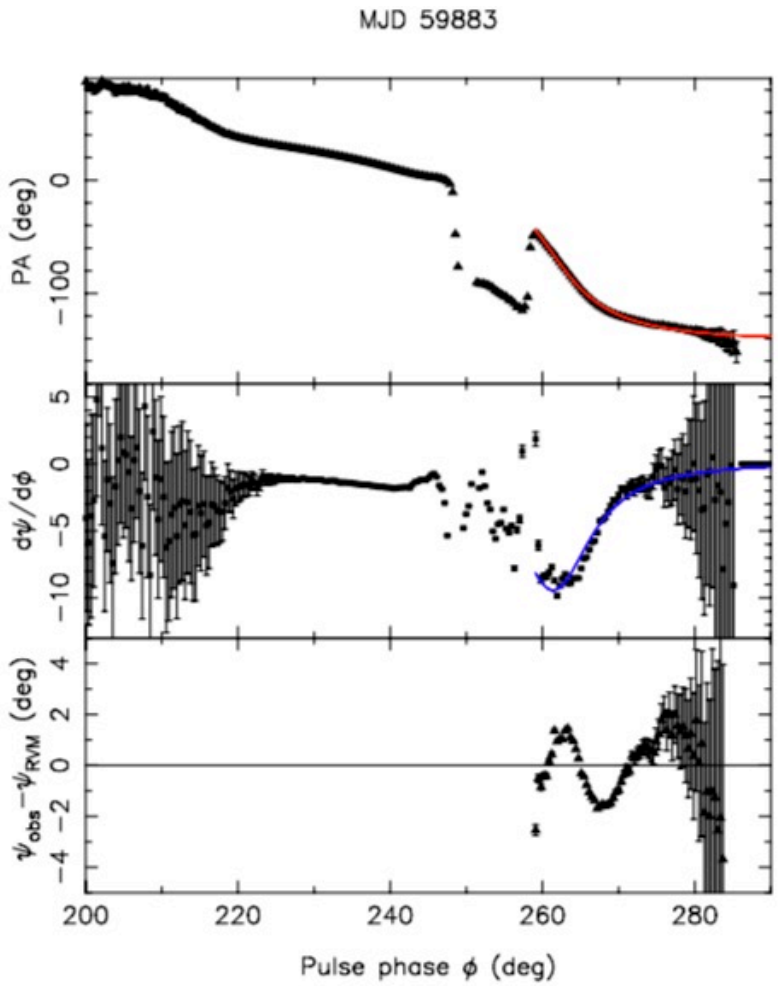


**Figure 19.** The RVM-fit based on observed PA at MJD 59883.

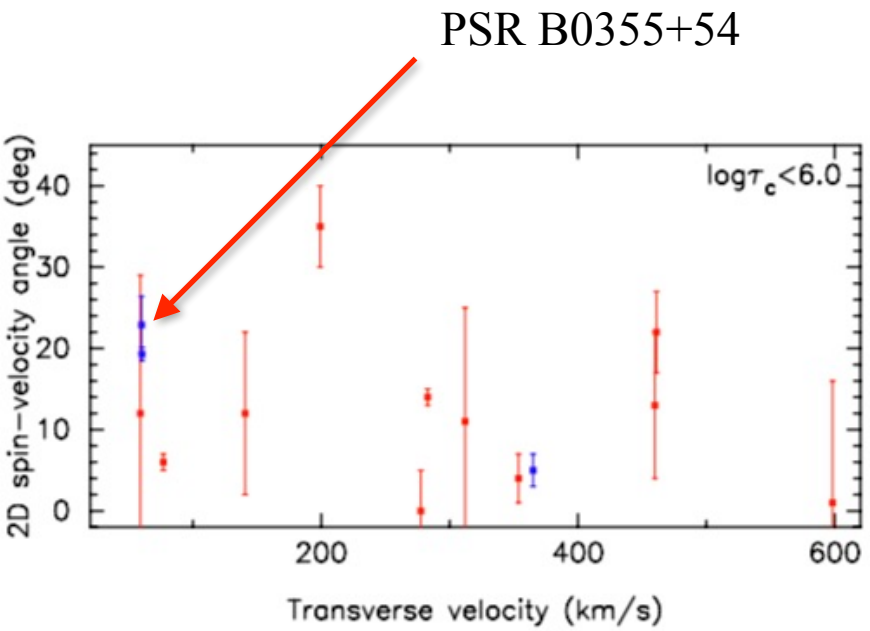


**Figure 20.** The 2D angle between spin and velocity.

| MJD | $\alpha$ (deg.) | $\sin\alpha/\sin\beta$ | $\psi_0$ (deg.) | $\phi_0$ (deg.) | $RM_{obs}$ (rad. $m^{-2}$) | $\psi_0$(intrinsic) (deg.) | $\psi_V$ (deg.) | $PA_{VPol}$ (deg.) |
|---|---|---|---|---|---|---|---|---|
| 59883 | 114.5±8.4 | −9.4±0.2 | −65.3 ± 1.5 | 261.4±0.2 | 82.160±0.002 | −288.8 ± 1.5 | 48.3±3.2 | 22.9±3.5 |

Blue points: from FAST;

Red points: from other telescopes;

Consistent with Janka's theory.

# Summary

## PSR B0355+54 and its PWN

- The D, PM and Pol of PSR B0355+54, and the long tail and stand-off radius of the PWN

## Interstellar scintillation of PSR B0355+54 from FAST

- **DS and ACF -** interstellar scintillation parameters vary with observing time
- **SS and small scale structure**- three ISS arcs; The movement of I, II and III.
- **Observations at 59881 and 59883** - interesting main arc and small scale structures.

## Polarization of PSR B0355+54 from FAST

- **Two modes** - mode A and B based on the detected PA; two modes have continuity in time.
- **2D spin-velocity angle** - updated 2D spin-velocity angle based on PA at mode B.

# Thank you!

# Propagation effects in the interstellar medium

- **The secondary spectrum**

→ Hill PhD thesis

$$\mathcal{L} = \frac{D_s}{\cos\theta_0} + \frac{D - D_s}{\cos\theta}.$$

Using small angle approximations and the binomial theorem,

$$\begin{aligned}\mathcal{L} &= D_s\left(1 + \frac{\theta_0^2}{2}\right) + (D - D_s)\left(1 + \frac{\theta^2}{2}\right) \\ &= (D - D_s)\frac{\theta^2}{2} + D_s\frac{\theta_0^2}{2} + D.\end{aligned}$$

Note that $D_s \tan\theta_0 = (D - D_s)\tan\theta$, so $D_s\theta_0 = (D - D_s)\theta$ for small angles. Thus

$$\begin{aligned}\mathcal{L} &= \frac{\theta^2}{2}\left(D - D_s + D_s\left(\frac{D - D_s}{D_s}\right)^2\right) + D \\ &= \frac{\theta^2}{2}(D - D_s)\frac{D}{D_s} + D \\ &= \frac{D\theta^2}{2}\left(\frac{1 - \beta}{\beta}\right) + D,\end{aligned}$$

where $\beta \equiv D_s/D$. The path length difference is therefore

$$\Delta\mathcal{L} = \mathcal{L}_2 - \mathcal{L}_1 = \frac{D}{2}\left(\frac{1 - \beta}{\beta}\right)(\theta_2^2 - \theta_1^2).$$

is the effective velocity of the pulsar (Cordes & Rickett, 1998).[6] The same Doppler shift then applies between the screen and the observer:

$$\nu_{\rm obs} = \left(\frac{1 + \boldsymbol{V}_{\rm eff,\perp}\cdot\boldsymbol{\theta}}{c}\right)\nu_e,$$

where $\nu_{\rm obs}$ is the observed frequency. The differential transverse Doppler shift between two points $\boldsymbol{\theta}_1$ and $\boldsymbol{\theta}_2$ in the image is thus given by

$$f_t = \frac{1}{\lambda\beta}(\boldsymbol{\theta}_2 - \boldsymbol{\theta}_1)\cdot\boldsymbol{V}_{\rm eff,\perp}, \qquad (1.4)$$

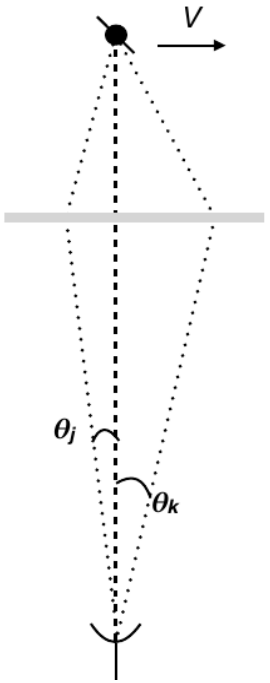


$$f_\nu = \eta f_t^2$$

$$\eta = 4625\frac{D_{\rm kpc}\, s(1 - s)}{\nu_{\rm GHz}^2 |V_{\rm eff,\perp}|^2}$$

← s, determine screen location

$$\boldsymbol{V}_{\rm eff,\perp} = (1 - s)\boldsymbol{V}_{\rm pulsar,\perp} + s\boldsymbol{V}_{\rm Earth,\perp} - \boldsymbol{V}_{\rm scr,\perp}$$

Dynamic spectrum(1.4 GHz, J0538+2817)

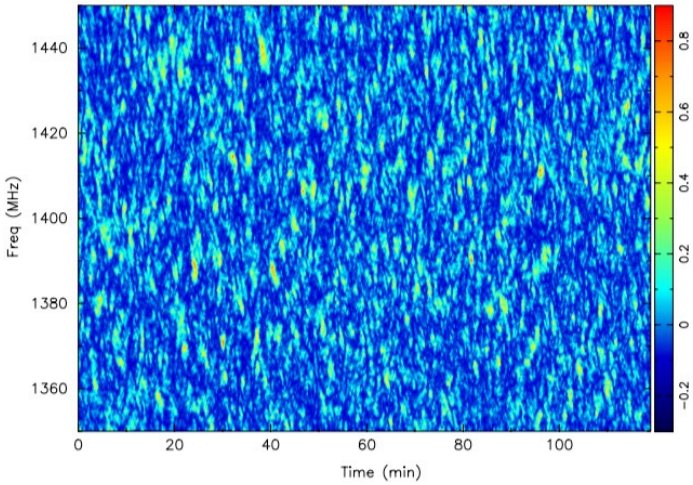


FT

Secondary spectrum(1.4 GHz, J0538+2817)